Article

Electrochemical Deposition of the Single Phase $Tl_xCu_{3-x}Se_2$ Thin Films

Francisco W. S. Lucas[a] and Lucia H. Mascaro[,a]*

[a]*Departamento de Química, Universidade Federal de São Carlos, 13565-905 São Carlos-SP, Brazil*

In spite of selenide semiconductors having a wide application area, $TlCu_2Se_2$ (TCSe) is poorly studied and its synthesis by non-vacuum or thermic methodology in film form is non-existent. Generally, the main problems of applying these TCSe compounds are related to complicated single phase growth, and the great time consuming and non-scalable fabrication method. In this work, the facile, fast, scalable and new electrochemical deposition of this material was proposed as a workaround for these main problems and obtaining single phase thin film. Thus, the electrodeposited $Tl_xCu_{3-x}Se_2$ films were characterized by scanning electron microscopy, X-ray diffraction (with Rietveld refinement) and energy dispersive X-ray spectroscopy. They showed interesting variation of composition (x =1.1, 1.2, and 1.25) and morphology as function of the electrodeposition potential, electrolytic bath temperature and thermal treatment.

Keywords: Cu_2TlSe_2, thallium copper selenide, electrodeposition, texturization, chalcogenide

Introduction

Ternary chalcogenides semiconductors are potentially attractive electronic materials and have been applied in solid state semiconducting devices, gas sensor and in many other areas.[1] In particular, copper thallium selenides are of interest for the development of advanced thermoelectric materials.[2] The crystals of $TlCu_2Se_2$ (TCSe) consist of layered structures, where the Tl^+ ions are located above and below the layers.[3,4] The unit cell can be seen in Figure 1.

It has been discussed that TCSe exhibits metallic properties and it possesses a relatively high conductivity ($\rho_{RT} = 5 \times 10^{-5}$ Ω cm).[3,5] To account for this behavior, Brun *et al.*[5] believed the conductivity was caused by the mixed-valence state of Tl^+ and Tl^{3+} in the lattice. However, it was demonstrated by Hall effect that this compound shows hole conductivity.[3,6,7] This fact rules out the existence of two oxidation state of thallium, because electrons would then fill the conduction band and act as charge carriers.[3,6] Ohtani *et al.*[7] investigated the electrical nature of $Tl_xCu_{3-x}Se_2$ (x = 1.1, 1.2 and 1.25) in more detail, concluding that conduction occurs predominantly by holes, but there is also a small contribution of electrons. A substantial difference was not observed between the conductivities measured for pressed powders and for single crystals of TCSe, which is indicative of a weak anisotropy of the crystals resistance.[3,6] Indeed, the electrical

*e-mail: lmascaro@ufscar.br
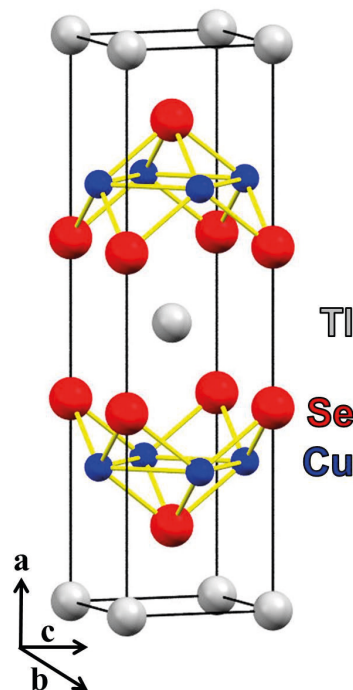
Figure 1. Unit cell of $TlCu_2Se_2$. For interpretation of the color references in the Figure, the reader is referred to the web version of this article.

and optical properties of group I-III-VI compound films are strongly related to the film growth techniques. TCSe has been prepared by heating, in sealed silica tubes in vacuum, stoichiometric amounts of TlSe, copper and selenium[3,4] or elemental mixtures at 500 ºC for 7 days. It is then formed into a pellet, and annealed at 250 ºC for

7 days, followed by slow cooling.[7] Moreover, as far as the authors know, the synthesis of TCSe film by non-vacuum or thermic methodology is non-existent. In addition to this, TCSe is poorly studied. Thus, we propose TCSe thin film preparation by electrodeposition, which is a facile, fast and new fabrication methodology for this compound.

Experimental

Chemicals and apparatus

The chemicals (analytical grade) were used directly without further purification. The following reagents were used: CuSO$_4$ (> 99.9%), Tl$_2$SO$_4$ (99.9995%), SeO$_2$ (99.9%), and H$_2$SO$_4$ (98%). Electrochemical experiments were performed in a potentiostat/galvanostat (PGSTAT 302N-Autolab, Metrohm-Eco Chemie). A three-electrode configuration electrochemical cell was used with a Mo or Pt plate (99.99%) as working electrode, a Pt plate as auxiliary and an Ag/AgCl/Cl$^-$$_{(sat. KCl)}$ as reference electrode. The composition and morphology of the films were evaluated by high-resolution field emission scanning electron microscopy (SEM; Zeiss Supra 35 FE-SEM) and energy dispersive X-ray (EDX) spectroscopy (FEI-XL30-FEG with an Oxford Instruments-Link ISIS 300 detector), respectively. The crystallographic films characterization was performed with the aid of an X-ray diffractometer (XRD; Rigaku, DMax2500PC) with CuKα radiation, counting time of 6 s and scanning step of 0.02°. The size of the crystallographic coherence dominium (D, in nm) was estimated from the (103) TCSe peak by the Scherer equation and the line broadening (instrumental effects) was corrected with silicon powder standard (99%, 325 mesh, SRM-640) using the Caglioti equation, as described by Gonçalves *et al.*[8] All samples were refined by the Rietveld method[9] through the General Structure Analysis System (GSAS) program.[10] The data available in the Inorganic Crystal Structure Database (ICSD)[11] were used as input for the theoretical model.

TCSe films deposition

Cyclic voltammetry (CV) was used to evaluate the electrochemical process of the elements and its mixture on Pt. The CVs were recorded at a scan rate of 50 mV s^{-1}, from 1.35 V *vs.* Ag/AgCl/Cl$^-$$_{(sat. KCl)}$ toward cathodic direction and, for deaeration, a stream of N$_{2(g)}$ was introduced into each solution for 10 min before each scan. Two potentials for electrodeposition of the TCSe films were chosen from these studies. Then, at a previously chosen more negative potential, different films were electrodeposited

using various electrolytic baths (EB) (with different ion concentrations) and analyzed by EDX. Thus, it was possible to choose the EB that formed films with composition close to the TlCu$_2$Se$_2$ phase. The temperature effect in film growth was studied at 25 and 50 °C, performing electrodeposition on Mo plate, using the optimized EB at each bath temperature and with total charge of 1 C (which resulted in ca. 1 h of deposition). Right before the electrodeposition, Mo substrate (1 cm^2) was cleaned ultrasonically with acetone, ethanol and H$_2$O/NH$_4$OH (1:1) during 10 min, in each solvent, then rinsed with deionized water and dried in an N$_{2(g)}$ stream. Thus, a 2^2 factorial design was performed with two liberty levels for electrodeposition potential and EB temperature. In an attempt to observe the effect of the annealing, a film obtained in one of the experimental levels was annealed during 1 h in Se atmosphere and different temperatures (150, 250 and 350 °C), with a heating/cooling rate of 5 °C min^{-1}. The film was placed into a lead borosilicate glass cylinder (sample cylinder, volume of 300 mL) and the partial pressure of the Se$_{(g)}$ was controlled by means of a crucible with 0.2 g selenium powder placed into this cylinder, which was not totally gas-tight (Figure 2). For this thermal treatment, a tube furnace was used and the atmosphere outside the sample cylinder was maintained at 1 atm of N$_{2(g)}$ and this gas exited the tube furnace through a bubbler filled with mineral oil with flow of 1 mL min^{-1}.
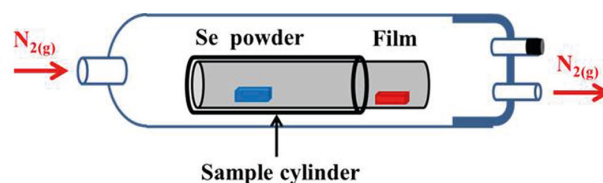

Figure 2. Thermal treatment apparatus: tube furnace, sample cylinder, film and Se sacrificial powder.

Results and Discussion

Electrochemical behavior

The electrochemical behavior of Pt electrode in 1 and 3 mmol L^{-1} of Cu^{2+}, 8 mmol L^{-1} Tl$^+$, and 1 mmol L^{-1} of H$_2$SeO$_3$ with supporting electrolyte (SE), 0.5 mol L^{-1} Na$_2$SO$_4$/H$_2$SO$_4$ and pH 2, was separately studied and the voltammograms are presented in Figure 3.

In Figure 3a, the voltammograms for solutions containing 1 mmol L^{-1} (red dashed curve) and 3 mmol L^{-1} CuSO$_4$ (blue dotted curve), and for blank solution (only SE; black solid curve) can be observed. A well-known electrochemical behavior of the Pt substrate in 0.5 mol L^{-1} Na$_2$SO$_4$/H$_2$SO$_4$ and pH 2 (SE) was seen with peaks corresponding to hydrogen adsorption and desorption (0.0 to –0.3 V), and to
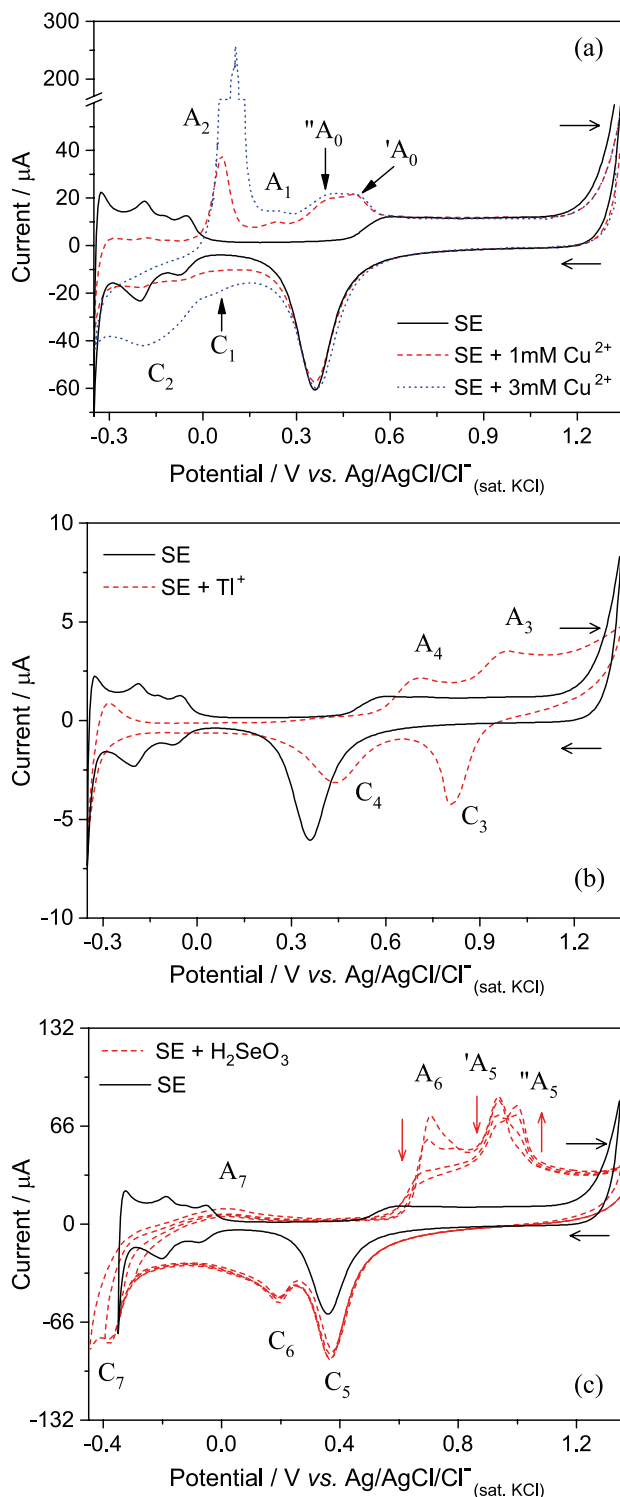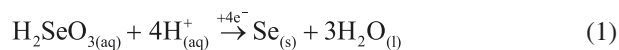
Figure 3. Room temperature cyclic voltammograms on Pt and at scan rate of 50 mV s^{-1} for solutions: (a) 1 and 3 mmol L^{-1} CuSO$_4$; (b) 4 mmol L^{-1} Tl$_2$SO$_4$; and (c) 1 mmol L^{-1} H$_2$SeO$_3$ in 0.5 M Na$_2$SO$_4$/H$_2$SO$_4$ and pH 2 (SE).

the formation (> 0.5 V) and reduction (ca. 0.4 V) of PtO$_x$. In the presence of Cu^{2+}, two cathodic peaks (C$_1$ and C$_2$) and four anodic peaks ('A$_0$, "A$_0$, A$_1$ and A$_2$) appeared, and the peaks corresponding to hydrogen adsorption/desorption were

inhibited due to the Cu underpotential deposition (UPD) that occurs between 0.05 and 0.005 V (C$_1$), and the Cu bulk deposition attributed to C$_2$ peak. The anodic peaks can be attributed to the redissolution of Cu-bulk phases (peak A$_2$) and Cu-adatoms layers (peaks 'A$_0$, "A$_0$ and A$_1$). This behavior is largely known in the literature.[12-14]

In Figure 3b, we can clearly observe the redox pair C$_3$/A$_3$ (at ca. 0.81/ca. 0.98 V, respectively) which can be correlated to reduction/oxidation of the couple Tl^{3+}/Tl$^+$. In the studies of Shin *et al.*[15] on gold electrode, they observed the reduction/oxidation potentials for this couple in the same potential window as this work on Pt. Moreover, they observed two peaks for UPD of Tl on Au-(111) at –0.255 and –0.365 V. Herein, we attributed the peaks C$_4$/A$_4$ (at ca. 0.44/0.71 V) to Tl UPD on polycrystalline Pt electrode. The inhibition of the hydrogen adsorption/ desorption reaction agrees with this attribution; Tl-adatoms are blocking the Pt electrochemical sites. Figure 3c shows the voltammograms for Se species with different inversion potentials (E$_{inv}$ of –0.30, –0.35, –0.40 and –0.45 V). The selenium electrochemical behavior is well-known;[16-22] the C$_5$ (at ca. 0.37 V), C$_6$ (at ca. 0.19 V) and C$_7$ (at ca. –0.37 V) processes can be assigned to UPD, massive (bulk) deposition (equation 1) and to Se^0 (or H$_2$SeO$_3$) reduction to H$_2$Se$_{(aq/g)}$ (equation 2), respectively. In the reverse scan, the broad anodic peak A$_7$ (around 0.01 V) may be associated with oxidation of the H$_2$Se$_{(aq/g)}$ or H$_{2(g)}$ adsorbed at the electrode surface. The peak A$_6$ (ca. 0.71 V) is assigned to the dissolution of Se-bulk, and the 'A$_5$ (at ca. 0.94 V) and "A$_5$ (at ca. 1.00 V) peaks are for the dissolution of the first (Se on Pt) and last (Se on Se-adatom/Pt) Se layers, respectively. The dissolution peak area of the Se-bulk and last Se-adatoms layers decrease as long as the E$_{inv}$ become more negative (from –0.30 to –0.45 V), because these layers are also dissolved when Se is reduced to H$_2$Se. The increase in "A$_5$ peak area for more negative E$_{inv}$ may be evidence of a better organization of the Se-adatoms layer, which allows the use of all available Pt sites and increases the number of Se-adatoms in this layer.

$$H_2SeO_{3(aq)} + 4H^+_{(aq)} \xrightarrow{+4e^-} Se_{(s)} + 3H_2O_{(l)} \qquad (1)$$

$$Se_{(s)} + 2H^+_{(aq)} \xrightarrow{+2e^-} H_2Se_{(aq/g)} \qquad (2)$$

After that, the metals Cu^{2+} (Figure 4A) and Tl$^+$ (Figure 4B) were studied in the presence of H$_2$SeO$_3$ and then, the electrochemical profiles of all species together in solution (Figure 4C). Figure 4 shows the electrochemical behavior for the binary and ternary systems.

Comparing the individual electrochemical behavior of the species (shown in Figure 3) with the voltammogram of

the binary systems, we can identify the peaks associated with the formation of binary phases or the presence of
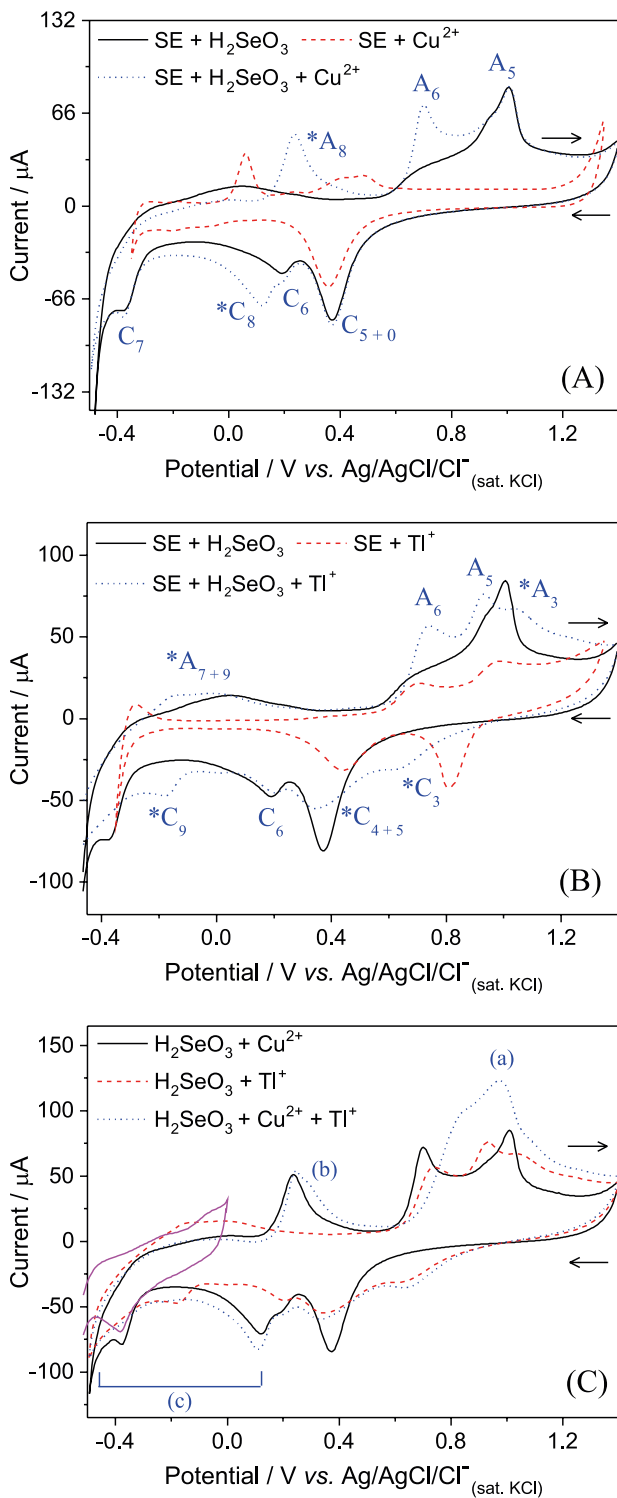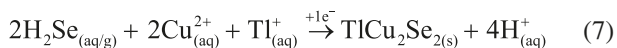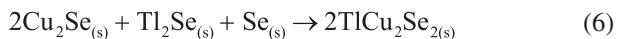

Figure 4. Room temperature cyclic voltammograms on Pt and at scan rate of 50 mV s^{-1} for the binary systems (A) 1 mmol L^{-1} CuSO$_4$ + 1 mmol L^{-1} H$_2$SeO$_3$ and (B) 4 mmol L^{-1} Tl$_2$SO$_4$ + 1 mmol L^{-1} H$_2$SeO$_3$; and for the ternary system (C) 1 mmol L^{-1} CuSO$_4$ + 4 mmol L^{-1} Tl$_2$SO$_4$ + 1 mmol L^{-1} H$_2$SeO$_3$ in 0.5 mol L^{-1} Na$_2$SO$_4$/H$_2$SO$_4$ at pH 2 (the first cyclic voltammogram scan on Mo is also shown for comparison).

a synergetic effect between the species. For example, in Figure 4A, it can be seen that the Cu presence increases the Se-bulk deposition or reduces its dissolution to H$_2$Se, which makes the A$_6$ peak area increase, compared to the individual behavior. The peak assigned as C$_{5+0}$ means that this peak can be a mixture of the individual processes C$_5$ and C$_0$. In turn, the new peaks *C$_8$/*A$_8$ can be associated with the deposition/dissolution of the Cu$_x$Se (x = 2 is most likely) phases (equation 3), as also described by other investigators.[16,23]

The voltammograms in Figure 4B show the electrochemical behavior for the Tl–Se binary system. The peaks *C$_3$/*A$_3$ are dislocated from the original potentials observed in the absence of Se, caused, perhaps, by Tl–Se layers adsorbed on Pt surface that add an additional resistance to the electrode. Comparing the voltammograms in the *C$_{4+5}$ region, we can see that the Tl-adatoms layer supress the Se-adatoms layer deposition, decreasing the peak area associated with C$_5$; however, the Se massive deposition does not seem to be affected by Tl$^+$ nor Tl-adatoms presence. In addition, a new peak was observed at about –0.2 V (*C$_9$) with oxidation peak merged with the C$_7$ peak (*A$_{7+9}$); these new processes can be attributed to the Tl$_2$Se deposition/dissolution (equation 5).

For the ternary system in Figure 4C, no new peaks were observed, but some of the voltammogram regions changed in relation to the binary systems. For clarity, the regions where noticeable changes were noted, letters from a to c were assigned. For example, the biggest change was viewed at region a; this variation could be resulted from the dissolution of the Cu–Tl–Se phase formed in forward scan, which takes place together with Se layers dissolution. The variation of the Cu–Se dissolution profile at region b can be associated with the small Tl incorporation into this phase. In turn, at region c, the peaks associated with the Tl–Se phase deposition (*C$_9$) and the H$_2$Se formation (C$_7$) were not observed. The increase in the current that starts at the Cu–Se phase deposition potential (*C$_8$), compared to the binary systems, is an indication that the Cu–Tl–Se phase is being formed. The growth of this phase may happen in three ways: by Tl incorporation into Cu–Se and Se phases at potentials more negative than *C$_8$ (equation 4); by the reaction between Se, Cu–Se and Tl–Se, for potentials lower than *C$_9$ (equation 6); and/or by the precipitation of Cu$^{+/2+}$ and Tl$^+$ with H$_2$Se (formed according to equation 2), for potentials below C$_7$ (equation 7). These three electrochemical/chemical mechanisms of deposition can be seen below:

$$Se_{(s)} + 2Cu^{2+}_{(aq)} \xrightarrow{+4e^-} Cu_2Se_{(s)} \tag{3}$$

$$Cu_2Se_{(s)} + Se_{(S)} + Tl^+_{(aq)} \xrightarrow{+1e^-} TlCu_2Se_{2(s)} \tag{4}$$

$$Se_{(s)} + 2Tl^+_{(aq)} \xrightarrow{+2e^-} Tl_2Se_{(s)} \qquad (5)$$

$$2Cu_2Se_{(s)} + Tl_2Se_{(s)} + Se_{(s)} \rightarrow 2TlCu_2Se_{2(s)} \qquad (6)$$

$$2H_2Se_{(aq/g)} + 2Cu^{2+}_{(aq)} + Tl^+_{(aq)} \xrightarrow{+1e^-} TlCu_2Se_{2(s)} + 4H^+_{(aq)} \qquad (7)$$

From the electrochemical behavior seen in Figures 3 and 4 and based on the proposed mechanisms, the potentials chosen for TCSe films electrodeposition were: –0.2 V ($TlCu_2Se_2$ deposition by mechanisms 4 and 6) and –0.4 V *vs.* Ag/AgCl/Cl$^-_{(sat.\ KCl)}$ ($TlCu_2Se_2$ deposition predominantly by mechanism 7). It is worth mentioning that the platinum electrode was chosen for such electrochemical behavior studies because of its well-known behavior and electrochemical/chemical stability. In the case of molybdenum (the substrate chosen for films deposition), its open circuit potential in this SE is around 0 V *vs.* Ag/AgCl/Cl$^-_{(sat.\ KCl)}$, which makes it impossible to study higher potential values, where this metal would be oxidized/dissolved. In contrast, Pt electrode has a great adsorptive character, showing great number of UPD depositions, which is not expected for Mo. However, in our study, at the potential region chosen for Cu–Tu–Se deposition, the mechanisms are dominated by massive depositions, which are not hugely affected by Pt adsorptive character, compared with Mo. For comparison, Figure 4C shows the cyclic voltammogram on Mo for the first scan in EB at the potential window where the Mo electrode is electrochemically stable. As can be seen in this Figure, there is no potential shift of the C_7 peak on Mo, compared to the same study on Pt. This observation was expected and corroborates our previous comments, since this process is associated with a massive deposition. After the first scan (not shown), the peak disappears, following the same behavior observed for Pt electrode.

From a previous study of the elements concentration in EB, the optimized constitution was: 1 mM $CuSO_4$, 4 mM Tl_2SO_4, 1 mM SeO_2 and 0.5 M Na_2SO_4/H_2SO_4 at pH 2 (supporting electrolyte). After that, the films were characterized by XRD (with Rietveld refinement; RR), SEM and EDX.

Films characterization

From 2^2 experiments, four different TCSe films were obtained and their surface morphology was studied using SEM (Figure 5). The films electrodeposited at –0.4 V and 25 or 50 °C were named as TCSe42 and TCSe45, respectively. Likewise, the films electrodeposited at –0.2 V and 25 or 50 °C were named as TCSe22 and TCSe25, respectively.
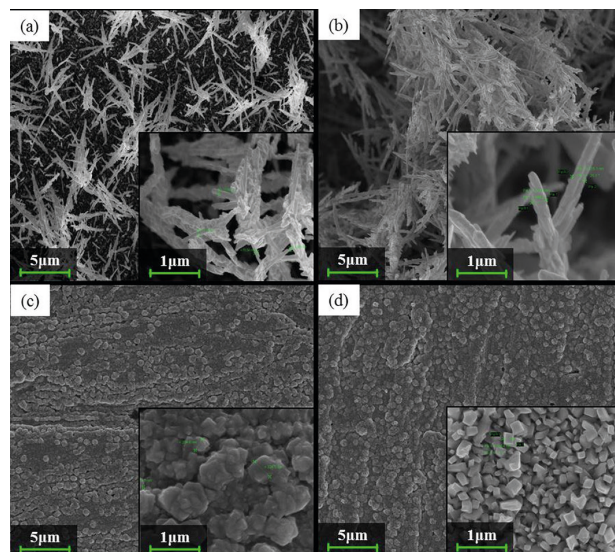
Figure 5. SEM micrographs with magnification of 100,000 and 10,000× of the films (a) TCSe42; (b) TCSe45; (c) TCSe22; and (d) TCSe25.

The film electrodeposited at –0.4 V and 25 °C (Figure 5a) showed a compact morphology with homogenously distributed structures like clusters of needles with medium diameter of about 70 nm. The increase of EB temperature to 50 °C (Figure 5b) made the cluster grow and coalesce. Comparatively, the films electrodeposited at –0.2 V (Figures 5c and 5d) had different morphologies, with smaller grains than those obtained at –0.4 V. The atomic composition of each film was evaluated by EDX and the contents are organized in Table 1. The estimate of the film thickness was based on the Faraday law with 100% efficiency and on its atomic composition; these data are also listed in Table 1.

The trend shown in Table 1 makes us conclude that the films composition was not significantly affected by the potential of deposition and bath temperature at the studied levels, with a standard deviation lower than 0.5% for triplicates. All deposited films showed Tl-rich/Cu-poor composition of the $TlCu_2Se_2$ phase; however, this change in Tl/Cu ratio does not interfere in the charge balance of the $TlCu_2Se_2$ crystals, since the Se–Se lamellae have oxidation state of –3 (–1.5 *per* Se atom) and both Tl and Cu atoms have oxidation state of +1, as observed by Folmer and Jellinek.[24]

In order to prove and identify the phase formation, RR was performed on TCSe films diffraction patterns. In Figure 6, the experimental and calculated XRD patterns are shown. The tetragonal unit cell parameters, the size of the crystallographic coherence dominium (D) and RR parameters of the films are shown in Table 2.

A good match between the experimental and calculated XRD patterns was observed, noted by the small R_{wp} value

**Table 1.** Approximate atomic composition of the films

Film	Cu / atom%	Tl / atom%	Se / atom%	Formula	Thickness[a] / μm
TCSe42	38	22	40	Cu$_{1.9}$Tl$_{1.1}$Se$_2$	1.05 ± 0.53
TCSe45	35	25	40	Cu$_{1.75}$Tl$_{1.25}$Se$_2$	1.08 ± 0.82
TCSe22	38	22	40	Cu$_{1.9}$Tl$_{1.1}$Se$_2$	1.07 ± 0.25
TCSe25	36	24	40	Cu$_{1.8}$Tl$_{1.2}$Se$_2$	1.07 ± 0.34

[a]Estimated from Faraday law with 100% efficiency, taking into account the composition and crystallographic parameters of each film listed in Table 2. The standard deviation for all elements is lower than 0.5 atom%. TCSe42 and TCSe45: films electrodeposited at –0.4 V and 25 or 50 ºC, respectively; TCSe22 and TCSe25: films electrodeposited at –0.2 V and 25 or 50 ºC, respectively.

Table 2. Rietveld refinement (RR) and tetragonal unit cell parameters (for better visualization, see Figure 1) and the size of the crystallographic coherence dominium (D) of the TCSe films

Film	RR parameter			Cell parameter			D[a] / nm
	R$_{wp}$ / %	R$_{Bragg}$ / %	χ^2	$a = b$ / Å	c / Å	V / Å^3	
TCSe42	25.13	8.79	1.253	3.8698	13.9604	209.062	17.82
TCSe45	16.81	8.35	2.027	3.8828	14.0365	211.613	30.31
TCSe22	25.85	14.07	1.777	3.8858	14.0085	211.517	23.20
TCSe25	20.60	20.44	1.073	3.8816	13.9938	210.840	24.20

[a]Estimated from the (103) TCSe peak. RR: Rietveld refinement; R$_{wp}$: weighted-profile Rietveld factor; R$_{Bragg}$: reflection intensity-based Rietveld factor; χ^2: chi-squared (related with the goodness of fit); a, b and c: lattice parameters; V: volume; D: crystallographic coherence dominium; TCSe42 and TCSe45: films electrodeposited at –0.4 V and 25 or 50 ºC, respectively; TCSe22 and TCSe25: films electrodeposited at –0.2 V and 25 or 50 ºC, respectively.
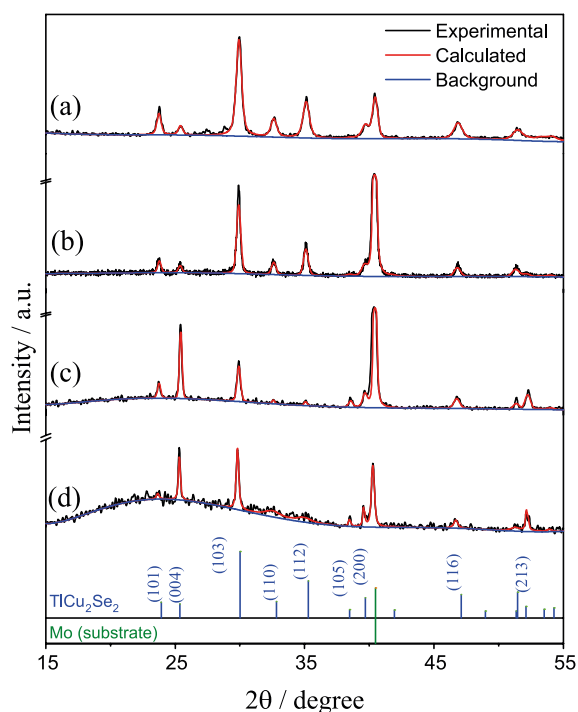

Figure 6. Experimental and calculated X-ray diffraction patterns of the films (a) TCSe42, (b) TCSe45, (c) TCSe22 and (d) TCSe25. Standard diffraction patterns for TlCu$_2$Se$_2$ (ICSD code 629124) and Mo (ICSD code 52267) phases can be seen at the graph bottom. For interpretation of the color references in the Figure, the reader is referred to the web version of this article.

(Table 2) and variation along the diffraction angle, as shown in Figure 6. Thus, by comparison with standard non-texturized TlCu$_2$Se$_2$ (space group I 4/m m m, ICSD code 629124) pattern available in the ICSD,[11] it was proven that all films were single phase TlCu$_2$Se$_2$. Also, some of the peaks were attributed to Mo substrate (associated with the ICSD code 52267 standard, space group I m-3 m). Comparing the relative intensities of the peaks (004) and (103) with those from standard non-texturized TlCu$_2$Se$_2$, we can conclude that the films electrodeposited at –0.4 V did not show texturing phenomenon. On the other hand, those electrodeposited at –0.2 V presented a notable increase in the number of domains with the TlCu$_2$Se$_2$ [004] crystalline plane oriented parallel to the substrate surface, noticed by the increase in the (004) peak intensity relative to the (103) peak. This texturization can also be associated with the morphology seen in Figure 5d.

Based on D values organized in Table 2, it was interesting to observe that the increase in EB temperature noticeably improved the films crystallinity for films deposited at –0.4 V, while only a small improvement was observed for those deposited at –0.2 V. These aforementioned observations make us probe that TlCu$_2$Se$_2$ growth mechanism is different for each deposition potential applied. For potentials more negative than –0.4 V *vs.* Ag/AgCl/Cl$^-$(sat. KCl), the H$_2$SeO$_3$

(or Se⁰) species are electrochemically reduced to H_2Se. This Se^{2-} source can chemically react with the metals (Tl and Cu) in solution, precipitating as non-texturized $TlCu_2Se_2$ (insoluble salt) on the electrode surface. The $H_2Se_{(g/aq)}$ solubility/concentration is strongly affected by the EB temperature, explaining the high effect of this parameter in the film crystallinity. In turn, the mechanism for electrochemical deposition at –0.2 V involves reaction in solid phase of elemental Se^0 with the metal ions (or Cu_ySe_x with Tl^+ ions) to grow the $TlCu_2Se_2$ compound. This last growth phenomenon is less affected by temperature and more surface confined than the first one, which can explain the fact that the films electrodeposited at this potential are texturized and their crystallinity are less influenced by EB temperature. Other authors proposed similar mechanisms for the In–Cu–Se system.[20-22]

Finally, the less crystalline film, TCSe42, was chosen to study the annealing effect on the material crystallinity, crystallographic phase, composition and morphology. Thus, this film was annealed at 150, 250 and 350 °C in Se atmosphere during 1 h. The effect of this treatment on surface morphology and composition can be seen in Figure 7.
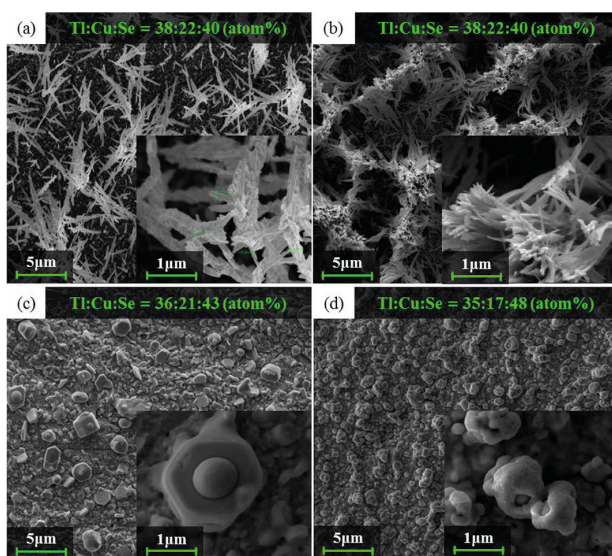
Figure 7. SEM micrographs of the TCSe42 film (a) as-deposited; and annealed at (b) 150, (c) 250 and (d) 350 °C.

From Figure 7, we observe a marked change on film surface with thermal treatment. The annealing at 150 °C (Figure 7b) did not change the film composition, but caused the increase of the number of clusters of needles, as well as change in the needle shape. This behavior can be associated with sublimation and condensation of $TlCu_2Se_2$ in Se vapor atmosphere during the annealing, which changed the needle shape and density. It is worth mentioning that the decrease

of film crystallinity after annealing in Se atmosphere was not expected, since the crystallinity of a great variety of selenide semiconductors has been improved after such treatment.[22,25] On other hand, from 150 to 250 °C, the clusters melt and Tl begins to sublime, while the films treated at 250 and 350 °C (Figures 7c and 7d) do not have clusters and the Se content increases. To observe any phase transition during these thermal treatments, the films were characterized by XRD. The diffraction patterns as a function of annealing temperature can be seen in Figure 8.
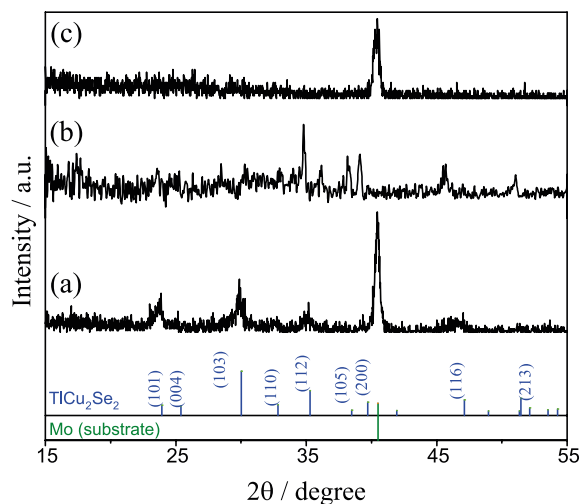
Figure 8. Experimental X-ray diffraction patterns of the TCSe42 films thermally treated at (a) 150, (b) 250 and (c) 350 °C. Standard diffraction patterns for $TlCu_2Se_2$ (ICSD code 629124) and Mo (ICSD code 52267) phases can be seen at the graph bottom.

As the diffraction peaks showed low intensity, close to noise level, it was not possible to perform the RR on diffraction patterns of the thermally treated films. However, it was possible to roughly estimate that the size of the crystallographic coherence dominium of the TCSe42 film annealed at 150 °C is almost half the as-deposited one, despite the annealed film seeming to be single phase $TlCu_2Se_2$. Thus, we can conclude that the thermal treatment at temperatures above 150 °C reduces the crystallinity of the films. Additionally, the films annealed at 250 and 350 °C were almost amorphous, making any phase identification difficult. Nevertheless, based on the composition, we believe that as long as Tl sublimes from the films they become amorphous Cu_xSe.

Conclusions

The electrodeposition of a good quality single phase $Tl_xCu_{3-x}Se_2$ with different compositions (x = 1.1, 1.2 and 1.25), morphology, crystallinity and crystallographic texturization was achieved. An interesting variation

of morphology as a function of the electrodeposition potential, the electrolytic bath temperature and thermal treatment was observed. The films electrodeposited at –0.2 V *vs.* Ag/AgCl$_{(sat. KCl)}$ were texturized with [004] crystallographic planes parallel to substrate surface, which could be related to observed tetragonal morphology.

Generally, the main problems of applying these TCSe compounds are related to the complicated growth of a single phase, the great time consumed and non-scalable fabrication method. In this work, using a facile, fast, scalable and new methodology these main problems were solved and it was possible to obtain a single phase $Tl_xCu_{3-x}Se_2$ (x = 1.1, 1.2 and 1.25) thin film.

Acknowledgments

References

1. Makovicky, E.; *Rev. Mineral. Geochem.* **2006**, *61*, 7.

2. Matsumoto, H.; Kurosaki, K.; Muta, H.; Yamanaka, S.; *J. Electron. Mater.* **2009**, *38*, 1350.

3. Starodub, V. A.; *Russ. Chem. Rev.* **1999**, *68*, 801.

4. Klepp, K.; Boller, H.; *Monatsh. Chem.* **1978**, *109*, 1049.

5. Brun, G.; Gardes, B.; Tedenac, J. C.; Raymond, A.; Maurin, M.; *Mater. Res. Bull.* **1979**, *14*, 743.

6. Berger, R.; Van Bruggen, C. F.; *J. Less-Common Met.* **1984**, *99*, 113.

7. Ohtani, T.; Taniguchi, M.; Sasaki, S.; Kishi, H.; Nakata, T.; *J. Alloys Compd.* **2004**, *383*, 245.

8. Gonçalves, N. S.; Carvalho, J. A.; Lima, Z. M.; Sasaki, J. M.; *Mater. Lett.* **2012**, *72*, 36.

9. Young, R. A.; *Rietveld Method*; Oxford University Press: London, 1995.

10. Larson, A. C.; Von Dreele, R. B.; *General Structure Analysis System (GSAS)*; Los Alamos National Laboratory Report LAUR 86-748, 1994.

11. https://www.fiz-karlsruhe.de/de/leistungen/kristallographie/icsd.html, accessed in June 2018.

12. Danilov, A. I.; Molodkina, E. B.; Polukarov, Y. M.; Climent, V.; Feliu, J. M.; *Electrochim. Acta* **2001**, *46*, 3137.

13. Molodkina, E. B.; Danilov, A. I.; Feliu, J. M.; *Russ. J. Electrochem.* **2015**, *56*, 999.

14. Marković, N. M.; Grgur, B. N.; Lucas, C. A.; Ross, P.; *Electrochim. Acta* **1998**, *44*, 1009.

15. Shin, J. W.; Bertocci, U.; Stafford, G. R.; *J. Phys. Chem. C* **2010**, *114*, 17621.

16. Steponavičius, A.; Šimkūnaitė, D.; *Russ. J. Electrochem.* **2002**, *38*, 488.

17. Santos, M. C.; Machado, S. A. S.; *J. Electroanal. Chem.* **2004**, *567*, 203.

18. Kemell, M.; Saloniemi, H.; Ritala, M.; Leskelä, M.; *Electrochim. Acta* **2000**, *45*, 3737.

19. Beni, V.; Collins, G.; Arrigan, D. W. M.; *Anal. Chim. Acta* **2011**, *699*, 127.

20. Lucas, F. W. D. S.; Lima, A. R. F.; Mascaro, L. H.; *Electrochim. Acta* **2014**, *147*, 47.

21. Lucas, F. W. S.; Mascaro, L. H.; *ECS Trans.* **2013**, *58*, 355.

22. Lucas, F. W. D. S.; Lima, A. R. F.; Mascaro, L. H.; *RSC Adv.* **2015**, *5*, 18295.

23. Šimkūnaitė, D.; Ivaškevič, E.; Kaliničenko, A.; Steponavičius, A.; *J. Solid State Electrochem.* **2005**, *10*, 447.

24. Folmer, J. C.; Jellinek, F.; *J. Less-Common Met.* **1980**, *76*, 153.

25. Costa, M. B.; de Souza Lucas, F. W.; Mascaro, L. H.; *ChemElectroChem* **2017**, *4*, 2507.